Computers in Biology and Medicine 141 (2022) 105135

Contents lists available at ScienceDirect

Computers in Biology and Medicine

journal homepage: www.elsevier.com/locate/compbiomed

Modeling the protective role of human eyelashes against ultraviolet light exposure

Michele Marro [a,*], Laurent Moccozet [a], David Vernez [b]

[a] University of Geneva, Centre Universitaire d'informatique, Battelle, Batiment A, 7 Route de Drize, 1227, Carouge, CH, Switzerland
[b] University of Lausanne, Center for Public Health and Primary Care Medicine (Unisanté), 44 Rue du Bugnon, 1011, Lausanne, CH, Switzerland

ARTICLE INFO

Keywords:
ocular exposure
Sunlight protection
Eyelashes
UV
Numerical model
Numerical simulation

ABSTRACT

The role of eyelashes in ocular radiation protection has been hypothesized for some time. There is however no quantitative knowledge of the shading they provide. The ocular protection provided by eyelashes is investigated in this study. A numerical model able to simulate an arbitrary source of light to illuminate a 3-dimensional head model with realistic details was used for this purpose. The eyelashes' filtering effect was studied for various light incidence angles, diameter and density of cilia. Using average values provided by literature to define their characteristics, we found that eyelashes reduce ultraviolet light received by the cornea by about 12–14%, with maximum values of 24%. These results suggest that the eyelashes can be an important element of the human eye protection system and their role should be further investigated.

1. Introduction

Eyelashes are a distinctive trait of mammals and similar features can be also noted in few species of birds and reptiles. They can change in structure, length, density and shape, suggesting that this is the result of a selection process and that these attributes correspond to specific needs now or in the distant past [1]. It has also been suggested that these attributes are correlated with the environmental context for each specific species. While their function is not yet elucidated, various hypotheses have been postulated about their role. It has been proposed that eyelashes protect the eye surface from dust, wind and light. They also facilitate the detection of close objects potentially dangerous for the eyes, producing an involuntary blink [1].

During the last decades eyelashes have become a field of interest from ophthalmology point of view and some studies have further investigated their characteristics. A previous study showed, through a physical model and tests in a wind tunnel, how mammals' eyelashes length is related to the eyes width and how this length is optimized to reduce deposition of airborne particles and to minimize evaporation of the tear film [2]. Another study further highlighted the importance of the eyelashes optimal length to reduce water evaporation, disregarding their direction and orientation [3].

There is little evidence on the role of the eyelashes in protecting the eye from radiation. Evidence of ocular shading was reported in a species of bird, noticing that a tiny layer of distanced fibers can stop a portion of light and protect the eyes [4]. In humans, longer eyelashes were observed in patients with Vernal Keratoconjunctivitis compared to healthy patients. The authors of the study hypothesize that this is a defense mechanism against factors promoting Keratoconjunctivitis, such as sun exposure, wind and foreign particles [5], presuming therefore a correlation between ocular exposure to solar radiation and protective role of eyelashes.

Although some authors have put forward this implication, such as [6–8], it remains essentially speculative. Arguably, however, the role of hair, which is similar in structure to eyelashes, in protecting the face from the sun is known. In particular, head hair was shown to effectively protect against solar ultraviolet radiation, with protection factors of 5–7 depending on the solar zenith angle [9]. It was also shown that facial hair (beard and mustache) reduces exposure to ultraviolet light by approximately one-third [10]. The level of protection offered by hair according to its density, thickness and the presence of melanin was further investigated by deGalvez [11], who notes the importance of the role of hair in protection against UV-A and UV-B.

Knowing and understanding the true role of eyelashes with respect to ocular exposure to ultraviolet radiation could be of considerable importance for the entire field dealing with adverse effects caused by this radiation, largely studied in literature [12].

The present study investigates, through modeling, the role of

* Corresponding author.
E-mail addresses: michele.marro@unige.ch (M. Marro), laurent.moccozet@unige.ch (L. Moccozet), david.vernez@unisante.ch (D. Vernez).

https://doi.org/10.1016/j.compbiomed.2021.105135
Received 27 August 2021; Received in revised form 27 November 2021; Accepted 10 December 2021
Available online 18 December 2021

eyelashes in ocular radiation protection. Shading mechanisms are formalized to examine the extent to which light received by human cornea is reduced by the presence of cilia. All results are obtained by performing virtual experiments using a numerical model able to predict light received by a 3-dimensional virtual object under an arbitrary condition of illumination.

2. Methodology

The general procedure adopted in this work to determine the eyelashes' filtering effect is to compare light received on human cornea with and without eyelashes. In this work, the word *filter* describes a component which, when crossed by a light beam, reduces its intensity. The filtering amplitude can be defined as

$$\alpha = \frac{I_R}{I} \quad , \tag{1}$$

where I_R and I stand for reduced intensity and intensity, respectively, received by a captor under the same condition of illumination. They represent irradiance (W/m^2), radiant flux (W), radiant dose (J/m^2) or any radiometric quantities derived, with and without the filter, respectively. The dimensionless variable α can take values in the interval [0, 1] and indicates how much light gets through the filter. Extreme values are $\alpha = 1$ which means that there is not filtering effects ($I = I_R$), and $\alpha = 0$ which means that the whole light is stopped.

All experiments are "virtually" carried out by a numerical model able to simulate an appropriate light source and detect how this light is received by a complex 3-dimensional virtual object (detailed explanation in Section 3.1). Every virtual object used in the numerical model is composed by meshes of flat triangles that approximate the shape of a real object. The higher the number of triangles, the closer the object is to the real object.

In this work, a realistic human head model is used as 3-dimensional virtual object (here after called head model) with realistic eyes designed from data in the literature (detailed explanation in Section 3.2) and approximated virtual eyelashes (detailed explanation in Section 3.3).

To facilitate the measurement process, the experiment is divided in two different parts, keeping the same final target. The first experiment consists in determining the amplitude of the filter (i.e. Equation (1)) for eyelashes in relation to their parameters (e.g fibers density, fibers diameter) and light (direction) without considering the filtering effect on the cornea. This procedure aims to represent the filter in the form of an equation. The advantage of doing this is firstly to avoid doing simulations with a head model with detailed eyelashes, potentially too heavy for model efficiency and computational resources of simulations. Secondly, a filter in the form of an equation facilitates sensitivity experiments for various eyelashes. Furthermore, there may be a simple interest to merely know the filtering effect of eyelashes. The second experiment consists in determining the light finally received by the cornea surface, implementing the result of the first experiment. In this step, eyelashes are represented by simple triangles, instead of realistic fibers, carefully designed on the head model. Intensity of light rays changes according to triangles interactions and it is described through the previously determined equation, reproducing a realistic effect of filtering.

The action of the filter on the human cornea is represented in terms of diffuse radiation view factor [13]. Diffuse radiation view factor is calculated through numerical integration for each cornea finite element (represented by a triangle mesh) and it represents the portion of radiation that reaches each triangle. The radiation source is represented, for each triangle, by a hemisphere of constant-intensity light. Light rays are emitted from the corresponding hemisphere which is centered in each triangle's center and orientated toward the perpendicular to the surface (the normal vector). The total number of light rays for each hemisphere is 10^5. The numerical integration takes into account orientation, shadows due to other triangles and, clearly, filtering effect of eyelashes. The maximum value is 1 and this means that the triangle receives light from the whole corresponding hemisphere. The value of 0 means that the triangle is completely in shadow.

3. Modeling

3.1. The numerical model

The numerical model used in this experiment is a rewritten and improved implementation of SimUVEx [14,15]. SimUVEx is used as a tool to predict ultraviolet radiation received by human skin. The model uses 3-dimensional virtual objects (meshes) composed of many triangles which replicate an arbitrary posture of a person and real irradiance data (W/m^2) as input.

In this new implementation, SimUVEx has been taken as reference for rewriting a new model from scratch in Python language in a standalone modality (SimUVEx is a plugin of Meshlab software [16]), using optimized ray-tracing libraries that make it at least 10 times faster than before. In addition, a few algorithms have been improved to make the model more precise. For instance, the new implementation is able to estimate the visibility maps using about 10^5 points, instead of the 400 used in the original program, without resorting to a bounding sphere but only to a mathematical-based implementation.

Furthermore, light is detected by triangles' centers instead of the vertices as in SimUVEx, which has the advantage of that it is no longer necessary to approximate the normals and areas of each detection point (page *724* of [14]). The model's output has also been thought in line with the necessities of users. Now it is possible to visualize directly the distribution of light received on the 3-dimensional virtual object at any simulation timestep. This new functionality, which was not implemented previously, allows to better understand several interesting features such as spatial coverage of light, dynamic shadow mapping, and instantaneous dose received on the object.

3.2. Head and eye model

The head model used in this experiment is a realistic 3-dimensional head of a young man made up of about 15 000 triangles (detail of ocular region in Fig. 1-a). It does not represent an average head but rather a generic head with Caucasian traits. We are aware that results can be different from head to head because they can be affected by different individual facial features such as eyelids, forehead prominence, or eye position. The results presented here are for this particular head model. However, it is assumed that other head morphologies should not change the results to the extent that the conclusions of this study are altered.

The cornea is modeled as a classical aspherical surface without further terms of Taylor expansion. The conic constant is $k = -0.1$ and the radius is 7.76 mm (average values for a 30-year old men [17]). Aperture diameter is about 12 mm (real value is 11.77 mm [18] but due to the discretization it is approximated). The graphical representation of the eye is shown in Fig. 1-b. To avoid a not-uniform light sensitivity consequently a not-uniform subdivision of the cornea (light is detected by the center of the triangles), the cornea was initially modeled as geodesic polyhedron in order to obtain a quasi-uniform distribution of light receptors. Then a geometrical isometry has been applied to the vertices of the solid in order to make the geodesic polyhedron conic. Successively it was cut to have the desired aperture diameter. The geometrical isometry does not keep the quasi-uniform subdivision, because it alters the local density of receptors. However, it is a good compromise between an uniform subdivision and an ordinary subdivision of variables θ (zenith) and ϕ (azimuth). The total number of visible triangles of the cornea is about 10 000. The eyes are positioned in the head model according the measurements found in Ref. [19].

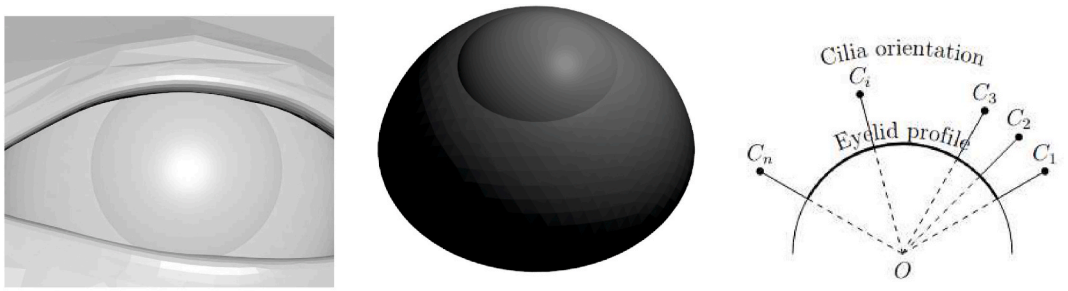

Fig. 1. Figure (a): detail of the head model used with eyelid contour, cornea and eyeball. Figure (b): 3-dimensional virtual eye placed in the head model. Figure (c): graphical representation of Equation (2) by taking a horizontal section of ocular region: O is the eye center and the eyelid profile is represented by a circular arc while C_i is the i-th center of eyelashes' triangles. From this last figure is clear that cilia have a normal direction to the eyelid profile.

3.3. Eyelash model

The eyelash is simplified to a periodical flat lattice of cylinders. Each cylinder, which represents a single fiber, is made up of 100 triangles. Cylinders have a diameter of d and a centre-to-centre distance of h, where $d \leq h$. Thanks to its symmetry the lattice can be described by only two vectors: a normal vector $\vec{e}_n$ and a transverse vector $\vec{e}_t$ (the vector transverse to the eyelashes' fibers).

A graphical representation of the lattice is shown in Fig. 2, together with an arbitrary light source I in order to show the angles that will be used later: θ (angle between light source direction and $\vec{e}_n$) and ϕ (angle between light source direction and vector $\vec{e}_t$).

In the head model eyelashes are represented by flat triangles. Each eyelash is made up of 6000 triangles.

4. Implementation

The optical phenomena that characterize the light and cilia interaction (absorption, transmission and reflection) depends on the type of light used and the material under examination. Studies on this interaction are however scarce, and it is not possible to have precise data that can be directly implemented in the model. To solve this drawback, we considered the great similarity between human eyelashes and hair in terms of structure [20] and anatomy [21]. Human hair has quite often been studied from an optical point of view, especially with regard to the phenomenon of transmission. It is for instance hypothesized that vellus hair may serve as an alternative pathway in the transmission of ultraviolet photons to stem cells and be a possible origin of melanoma after exposure to ultraviolet radiation [22,23]. Regarding the reflection phenomenon, however, only a few studies can be found (e.g. Refs. [24, 25], where infrared spectroscopy is used to determine structural information about hair). There are some models that, based on optics, simulate light-fiber interaction (such as [26–28], and [29]). However, they use the visible wave spectrum, since their ultimate goal is to create realistic virtual objects. Thus, the only validity regarding the performance of these models is aesthetic, which does not imply that it is also numerically correct.

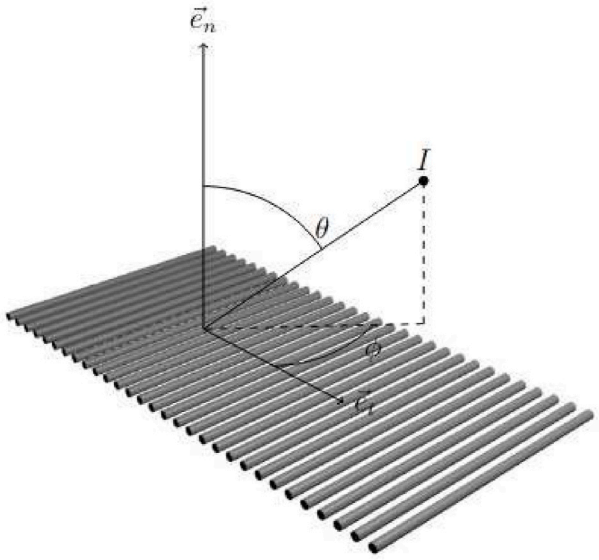

Fig. 2. Graphical representation of the lattice used in the virtual environment as eyelashes and its referent system.

The only data found involving spectral reflection measurements for hair are from a wavelength of 360 nm upwards. Around this range, reflection is characterized by a relatively low value, probably due to the strong absorption determined by the amount of melanin and its type, which in fact has an absorption spectrum that increases with shorter wavelengths. For example, the reflection in this range for brown hair found in Ref. [30] is around 2%, in Ref. [31] it is around 2.5–3.5%, and in Ref. [32], where light reflection measured from strands of brown hair, it is less than 4%. In Ref. [22] there is also a list of attenuation coefficients (expressed as the sum of absorption and scattering coefficients) derived from different studies, which are characterized by a high value for the short wavelength. In Ref. [33], the same trend is found.

In light of these data, it was decided to use a light source for which reflection can be neglected, namely an ultraviolet light source (more specifically the UV-A and UV-B interval, 280–400 nm), collimated for the first experiment, hemispherical (as explained in Section 2) for the second part. Eyelashes are considered, in terms of interaction with light, as dark hair. In terms of transmission, in Ref. [11] we find an almost constant value of about 20% sufficiently covering the considered wavelength range. Thus, the model implemented here models the optical properties of cilia through 80% absorption and 20% transmission.

For the first experiment (derivation of α without considering the effect on the cornea) light is detected by a well-defined area (represented by green color in Fig. 3), which represents a real sensor. It is located under the filter, with a size smaller than the filter itself to avoid registering light not filtered during the experiment and large enough to detect light through a sufficient number of fibers. The sensor is composed by about 12 000 triangles and consequently the same number of light receptors. Light is detected and registered by each receptor and the final value of total intensity received is the average value of intensity among the receptors. For uncertainty estimation an algorithm that take the receptors' position randomly on each corresponding triangle surface has been implemented [34]. This algorithm is used only in this configuration and allows to compute the variance as $\sigma^2 = \sum_{i=1}^{M}(I_i - \bar{I})^2/(M-1)$ where $\bar{I} = \sum_{i=1}^{M} I_i/M$ is the average value of light intensity received for each random case and I_i is the average value

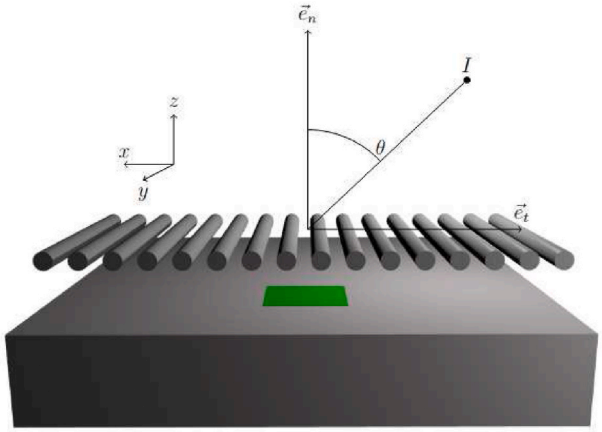

Fig. 3. Graphical representation of the first experiment to determine the filtering effect given a light source I along the axis $\vec{e}_t$ of direction θ.

of light intensity received among receptor for each random case. M is the number of simulations for each set of eyelashes parameters. In addition, it has been noticed that each error shows a Gaussian distribution.

The behavior of the filter can be illustrated with some specific examples. To simplify the configuration we can image a simple situation where light source illuminates the sensor only along the transverse direction of fibers (the x-axis in Fig. 3, or alternatively when $\phi = 0$). Because of the filter geometrical symmetry, a variation of light-source direction only along fiber direction (y-axis in Fig. 3) does not change the value of α. Therefore, for this configuration is reasonable to write that $\alpha = \alpha(\theta; d, h)$. It is also reasonable to expect that, for reasons of symmetry, the function α is an even function in this configuration ($\alpha(-\theta) = \alpha(\theta)$).

Taking into account an arbitrary direction of light source, instead, filter amplitude will clearly depend also on ϕ. It is reasonable to suppose that in the most general configuration $\alpha = \alpha(\theta, \phi; d, h)$. Moreover, the sign of $\vec{e}_t$ does not change the filter amplitude, and it can also be assumed that α is an even function also for the ϕ variable, so $\alpha(\theta, -\phi) = \alpha(\theta, \phi)$.

Thanks to the two vectors that can describe eyelashes orientation in space, we are able to orient the lattice on the head model to improve the virtual representation. In reality, eyelashes follow the eyelid curve and, consequently we can consider that fibers are roughly oriented along the vector radius centered on the eyeball center. To formally do this, we define the vector $\overrightarrow{OC_i}$, where O is the coordinate of the eyeball center, C_i is the coordinate of the i-th triangle center of the structure which represents eyelashes. Vector $\vec{e}_{n,i}$, the normal vector of the i-th triangle of eyelashes, is automatically defined by the virtual structure of eyelashes on the head model. Finally, $\vec{e}_{t,i}$ can be calculated as the orthogonal vector to the vector $\overrightarrow{OC_i}$ and $\vec{e}_{n,i}$. So, formally $\vec{e}_t$ is defined as

$$\vec{e}_{t,i} = \vec{e}_{n,i} \times \overrightarrow{OC_i} \quad , \tag{2}$$

where $\times$ is the vectorial cross product. A graphical representation of eyelashes orientation is shown in Fig. 1-c. This latter figure illustrates how the cilia have a normal direction to the eyelid profile. In this figure, a horizontal section of ocular region is schematically shown. The eyelid profile is represented by a circle arc and the eye center from the point O. Points C_i represent the center of the eyelashes' triangles. Because of Equation (2) cilia are always perpendicular to the eyelid profile.

In the second experiment an eyelash structure is built on the head model by using flat triangles. Diffuse radiation view factor is calculated for each cornea triangle, taking into account light ray filtered from this structure. Filtering amplitude is applied according to the light direction and filter trend derived in the next section.

5. Mathematical formulation of the filter

A mathematical formulation of the filter is not mandatory but useful to understand what kind of mathematical function (α) is expected from the first experiment. Additionally, after carrying out this experiment it is possible to compare the results obtained with the model and the derived function. The purpose of this is to ensure that the derived function can satisfactorily describe the trend of the filter, so that this function can be used directly for the second experiment. This process also avoids having to fit our data and find a relationship between fit parameters and eyelashes parameters (which may not be so obvious).

First of all, we would like to analyze the simple case where light illuminates the eyelashes structure from a direction transverse to the fibers (i.e. when $\phi = 0$). Fig. 4 represents a single interval of the periodical lattice onto the plane xz of Fig. 3, illuminated by a collimated light source of direction θ, such that $\theta \in [-\pi/2, \pi/2]$. For all conditions described in Section 4 filter amplitude can be formulated in terms of visible area between two contiguous fibers. Indeed, the quantity of light that the sensor can detect depends on the shadows area projected by the lattice, which in turn depends on the angle of illumination θ. Therefore, the ratio between light intensity with and without the filter is proportional to the ratio between visible area with and without the filter.

A more formal motivation of this can be expressed in terms of radiant flux received. Radiant flux received for a collimated light without the filter is proportional to the visible sensor area, which is smaller if the periodical lattice of cylinders covers it. The ratio between the first and the second case (e.g. to the function α) is therefore the ratio between the visible areas in these two configurations.

The filter being a periodic lattice, we can focus the study on one single interval and reduce the study to a one-dimensional problem. It is noted that the visible area is actually the distance between two parallel planes, internally tangent to a couple of fibers and parallel to the light direction, projected onto the plane of the sensor. Considering a reference frame centered in the left fiber's center of Fig. 4, with the tangency condition, the first tangent plane for left fiber is:

$$x\cos\theta - z\sin\theta - d/2 = 0 \quad , \tag{3}$$

whereas the second tangent plane for right fiber is

$$x\cos\theta - z\sin\theta - h\cos\theta + d/2 = 0 \quad , \tag{4}$$

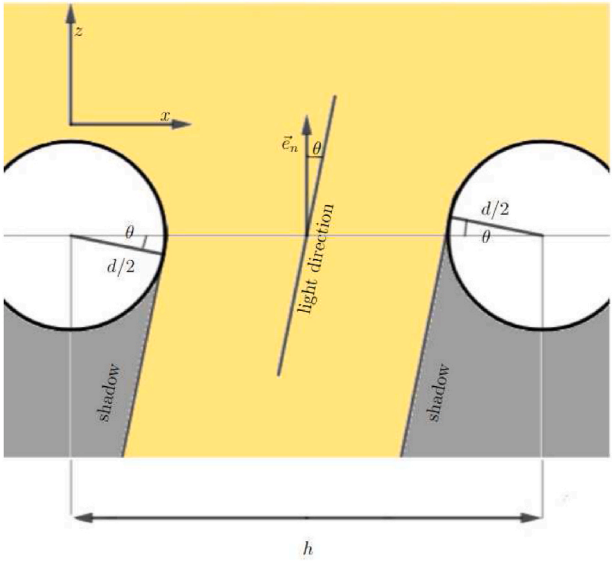

Fig. 4. Transverse section of the lattice illuminated from a collimated light source from a direction θ. Light has been graphically represented with yellow color while in grey the shadows projected from it.

clearly parallel to the first one. Perpendicular distance D_{perp} is

$$D_{perp} = h\cos\theta - d \quad . \tag{5}$$

The quantification of the transmission of light through the fibres can be obtained by considering that this is equal to the sum of the two fiber radius r multiplied by the transmission factor k_T. Therefore, the total visible area with the eyelashes, A_{filt}, also considering the absorbed part, can be written as

$$A_{filt} = D_{perp} + k_T d \quad . \tag{6}$$

This last equation is valid as long as $|\theta| \leq \cos^{-1}(d/h)$. For other values of θ we have a mix of filtered and double filtered light (thus proportional to a k_T^2 term) due to the perspective superposition of two contiguous fibers. The light will be filtered multiple times starting from when D_{perp} (which now is negative) assumes a value equal to $-d/2$, i.e. when $|\theta|. > \cos^{-1}(d/2h)$, which is also the value for which the minimum number of transmissions is two.

The treatment of multiple transmission is beyond this simplistic formulation, as well as the range of use of the numerical model. However, in order not to lose consistency, we can in any case determine a range of possible solutions. The filter for $|\theta| \leq cos^{-1}(d/h)$, being the visible area without the filter always $A_{nofilt} = h\cos\theta$, is described from the following equation

$$\alpha(\theta; d, h, k_T) = 1 - \frac{d(1-k_T)}{h\cos\theta} \quad . \tag{7}$$

The value of the filter in the extremes of this validity interval is always k_T. The filter amplitude, starting from this value, will decrease until it ideally reaches 0 at $\theta = \pm\pi/2$. So the "true" value of the filter is always between 0 and k_T for $\cos^{-1}(d/h) < |\theta| \leq \pm\pi/2$. We can then estimate the extremes of our range of possible solutions by considering $\alpha = 0$ as the maximum filtering (α_{max}) and $\alpha = k_T$ as the minimum filtering (α_{min}) for this reference interval. So the final general equation of the filter can be summarized as follows

$$\alpha(\theta; d, h, k_T) = \begin{cases} 1 - \dfrac{d(1-k_T)}{h\cos\theta} & |\theta| \leq \cos^{-1}\left(\dfrac{d}{h}\right) \\ 0 \quad \text{or} \quad k_T & \text{otherwise} \end{cases} . \tag{8}$$

The filter amplitude depends on, in particular, the ratio between the two parameters d and h, which can take values between 0 and 1 (k_T is always treated as a constant). In order to find out if the model results can satisfactorily be reproduced by Equation (8) for the interval of usability of the model, a virtual experiment using the same condition of illumination was implemented by using the numerical model. The periodical lattice of cylinders is illuminated in this instance by a collimated light source of unitary irradiance (W/m^2) from different values of θ, such that $|\theta| \leq \cos^{-1}(d/h)$, in order to estimate I_R. The experiment was carried out

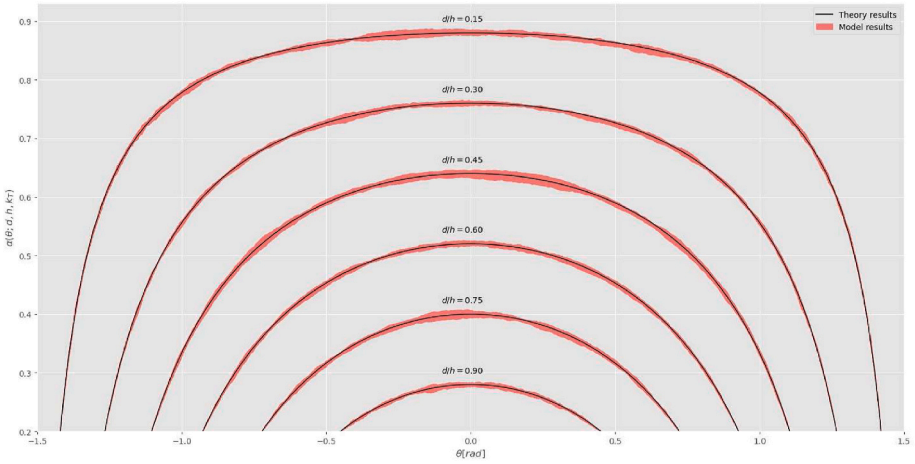

Fig. 5. Results of the model (red areas correspond to the 95% of the confidence interval) calculated in terms of α by using Equation (1) and Equation (8) (bold lines) for different values of θ, $\phi = 0$, the same set of pairs d and h, and $k_T = 0.2$.

Table 1
Fitting parameters, using the fit function $f(x) = a + bx$, according to Ref. [35]. First table shows the parameters obtained with the method of Least Squares by using Equation (8) as fit function. It shows also the total number of points (n) used in the fit (n varies with the configuration, because we only used non-zero values), the root mean square error (RMSE) and Pearson correlation coefficient ρ. The second table shows the fitting parameters obtained by using Equation (9) for different values of ϕ and the parameters of the first table.

d [mm]	h [mm]	d/h	a	b	n	RMSE	ρ
0.03	0.2	0.15	− 0.002 ± 0.003	1.000 ± 0.006	6584	0.002	0.999
0.06	0.2	0.3	− 0.002 ± 0.005	1.001 ± 0.004	3175	0.002	0.992
0.09	0.2	0.45	0.003 ± 0.007	0.995 ± 0.005	1982	0.002	0.992
0.09	0.15	0.6	0.008 ± 0.007	0.99 ± 0.03	1330	0.002	0.991
0.09	0.12	0.75	0.001 ± 0.002	1.00 ± 0.03	880	0.002	0.995
0.09	0.1	0.9	− 0.002 ± 0.002	0.99 ± 0.07	480	0.002	0.992

ϕ[degrees]	d/h	a	b	n	RMSE	ρ
0	0.5	− 0.002 ± 0.002	0.997 ± 0.002	1728	0.003	0.996
15	0.5	0.003 ± 0.003	1.003 ± 0.003	1789	0.004	0.997
30	0.5	0.002 ± 0.005	0.997 ± 0.009	1996	0.005	0.993
45	0.5	0.005 ± 0.003	0.999 ± 0.002	2444	0.002	0.994
60	0.5	− 0.007 ± 0.005	1.001 ± 0.002	3458	0.002	0.992
75	0.5	− 0.005 ± 0.004	1.001 ± 0.002	6681	0.003	0.995
90	0.5	0.002 ± 0.002	1.000 ± 0.002	9999	0.001	0.996

using six different values of d/h (0.15, 0.3, 0.45, 0.6, 0.75, 0.9) and repeated for each configuration without the filter to derive I.

Results of the model are calculated in terms of the dimensionless variable α by using Equation (1). They are shown in Fig. 5 for M = 10, superimposing also the plot of Equation (8) using the same values of θ and parameters d and h. In Table 1 the fitting results are shown using [35] as reference. It can be observed that Equation (8) can optimally reproduce the results of the model. For all six trends, the Pearson correlation coefficient is always greater than 0.99 and each set of regression parameters (a and b) responds positively to a hypothesis test with a line 1:1.

In order to take into account the variable ϕ, the previous process has to be reformulated for a light ray from an arbitrary direction. The only modification that changes in this new configuration is the tangency condition of two parallel internal planes and the arbitrary direction of light, whereas the entire formulation remains the same. The difference is the substitution $\theta \rightarrow \arctan(\tan\theta\cos\phi)$ in Equation (8). Defining $\beta_{\theta,\phi} = \beta(\theta, \phi) = \arctan(\tan\theta\cos\phi)$ Equation (8) becomes

$$\alpha(\theta,\phi;d,h,k_T) = \begin{cases} 1 - \dfrac{d(1-k_T)}{h\cos\beta_{\theta,\phi}} & |\beta_{\theta,\phi}| \le \cos^{-1}\left(\dfrac{d}{h}\right) \\ 0 \quad \text{or} \quad k_T & \text{otherwise} \end{cases} . \tag{9}$$

To apply the same process also for Equation (9) (i.e. evaluate this function with the model results), which becomes Equation (8) for $\phi = 0$, it was decided to keep the d/h ratio constant and vary the variable ϕ. The simulations performed with the model obviously demonstrate a periodicity in the results given the cosine dependence of the variable ϕ. Consequently, a reasonable range for this variable is between 0° and 90°. Choosing a range of θ values such that $|\beta_{\theta,\phi}| \le \cos^{-1}(d/h)$, seven different values of ϕ have been chosen (ϕ = 0°, 15°, 30°, 45°, 60°, 75°, 90°) to estimate again I_R with the filter and then I by using the same configurations without the filter. Model results calculated in terms of the dimensionless variable α by using Equation (1) are shown in Fig. 6 for M = 10, superimposing also the plot of Equation (9) and using the same values of θ, ϕ, and a constant value of d/h (0.5). In Table 1 the fitting results are shown. As in the previous case, Equation (9) fits well the results of the model. The Pearson correlation coefficient is again always greater than 0.99, and each set of regression parameters (a and b) responds positively to a hypothesis test with a line 1:1.

In conclusion, Equation (9) can satisfactorily describe the trend of the filter in the interval of usability of it (e.g. when there is only single transmission), which implies a correct analytical construction of the filter. Consequently, Equation (9) will be used for the second part of the experiment.

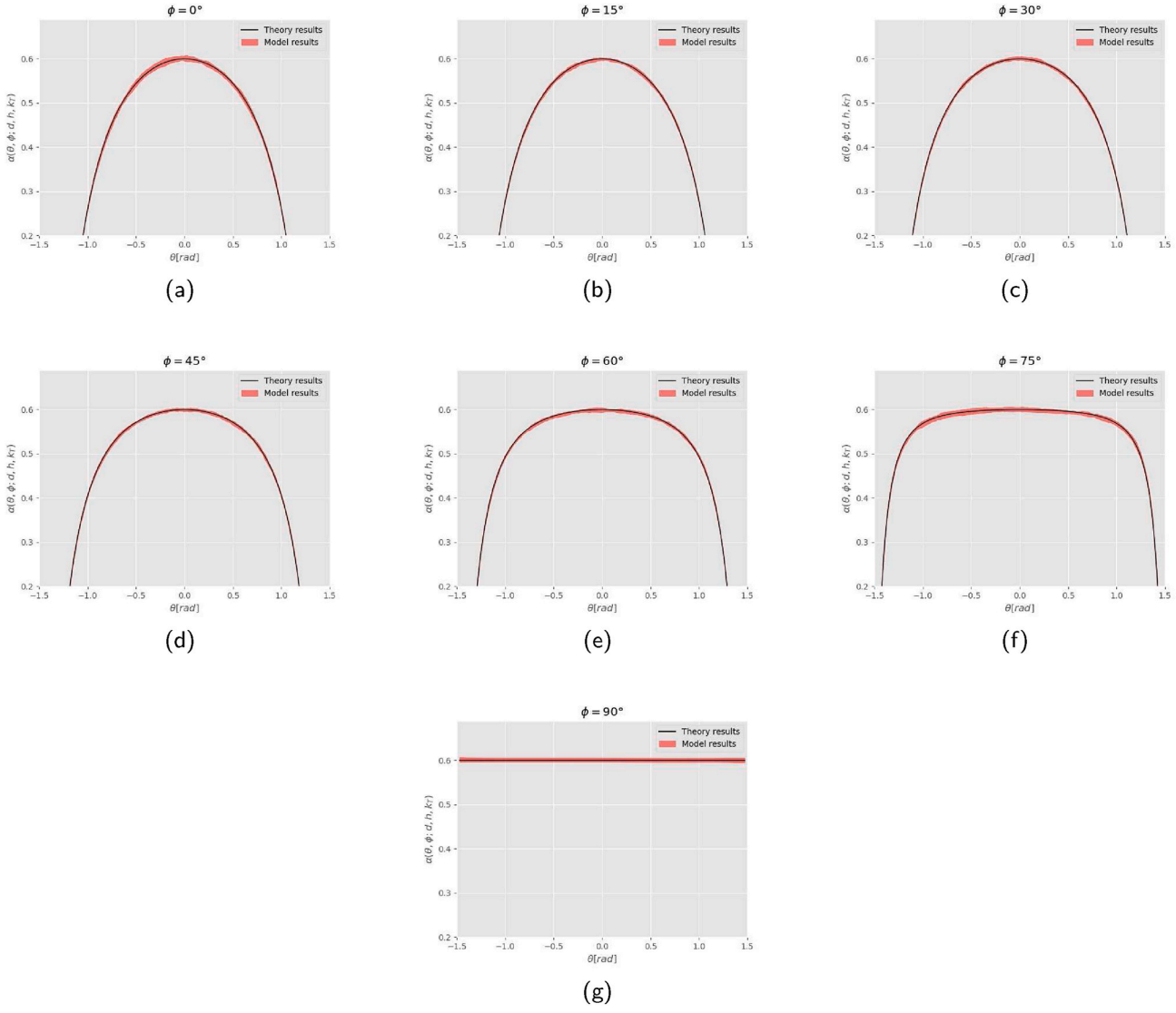

Fig. 6. Results of the model (red areas correspond to the 95% of the confidence interval) calculated in terms of α by using Equation (1) and Equation (9) (bold lines) for different values of θ, seven different values of ϕ, fixed value of d/h, and $k_T = 0.2$.

6. Results

First, we present the percentage difference for typical eyelashes values found in the literature, calculated through the $100\cdot(I - I_R)/I = 1 - \alpha$ formula, where I is unitary intensity of light without the filter, while I_R is with the filter, for minimum and maximum filtering. Then, through sensitivity experiments we investigate the behavior of filtering with different eyelashes values (ratio of d/h and length l).

According to Ref. [20], which population was composed by 29 Caucasian female, upper eyelashes length varies from 8 to 12 mm, even though rarely exceeds 10 mm, while lower eyelashes length varies from 6 to 8 mm. According to Ref. [36], which population was composed from 10 Caucasian female and 20 Asian female, there is not a significant difference in upper eyelashes length between these two population samples. Average length is about 7.1 mm. In Ref. [37], which population was composed of 50 Japanese people, no significant difference in upper eyelashes length was observed between gender. Average value is about 7.4 mm. This study reported however that both lower eyelashes length and density changed significantly between gender.The observed lower eyelashes' length was in average of 4.98 mm and 5.56 mm, while the eyelashes density was of 6 fibers per mm and 7.6 fiber per mm for men and women respectively. Another important value for this work is the fibers diameter, or thickness. Diameter of 71.7 μm and 61.0 μm were reported for Asian to Caucasian women, respectively [23,36]. In Ref. [38], which intended to build an apparatus similar to the eyelashes structure, an aluminum wire of 100 μm of diameter has been used as eyelashes fiber. Furthermore, in Refs. [36,37] average values of the eyelashes angle are reported.

For this work, we choose a length of 7 mm for upper eyelashes and a length of 5 mm for lower eyelashes. We considered an average eyelashes density of 7 fibers per mm (h = 0.143 mm) and a diameter of d = 65 μm ($d/h = 0.455$). For simplicity, the orientation of the eyelashes is always 90° compared to the vertical for both upper and lower eyelashes and density is always the same as well. All these values are reported in Table 2.

Due to the symmetry of the head model, we show the results only for the left eye (Fig. 7). Fig. 7-a shows the diffuse radiation view factor for left cornea without eyelashes. The upper and lower parts that appear cut off are due to the shading of the upper and lower eyelids. Indeed, the triangles of these two regions have a reduced visibility and the effect of the filter is not relevant. It shows how the view factor of diffuse radiation can reach values close to 1 in the region that is probably not affected by the shadow of the nose or the prominence of the eyelids and forehead.

Fig. 7-b represents diffuse radiation view factor with eyelashes (7 mm and 5 mm of length of upper and lower eyelashes, respectively) by using the filter equation with α_{max} for the left figure and α_{min} for right figure. The effect of the filter in this configuration, as compared to the first Fig. 7-a, is obvious. The diffuse radiation view factor is considerably reduced for both configurations. The effect of the filter is applied almost uniformly on the cornea region, except for regions close to upper and lower eyelid, where eyelids already stop the incoming light for both configurations acting as filter themselves. Diffuse radiation view factor is also reduced in the central-nasal part of the cornea, where the initial value was not as so high as in the central-temporal part. Moreover, the difference between minimum and maximum filtering is hardly noticeable. It can be seen that the figure representing the results using α_{min} has slightly higher values especially on the temporal-central part, near the border.

Fig. 7-c shows the percentage difference for each triangle of the cornea, calculated from the results shown in Fig. 7-a and the results corresponding of Fig. 7-b. Fig. 7-c on the left side is then the percentage difference between the results without the eyelashes and with the eyelashes parameterized using Equation (9) (and α_{max} for $|\beta_{\theta,\phi}| > \cos^{-1}(d/h)$). Similarly, Fig. 7-c on the right side is the percent difference between the results without the eyelashes and with the eyelashes parameterized using Equation (9) (and α_{min} for $|\beta_{\theta,\phi}| > \cos^{-1}(d/h)$). The percentage difference can reach values of approximately 24% for the results presented in the left figure and 20% for the results depicted in the right figure. These values are found for both configurations in the border region (nasal and temporal), and decreases toward the center. Unsurprisingly, since the two Fig. 7-b are very similar, little differences can be observed between the two Fig. 7-c. It is quite clear that the influence of the filter for values where the minimum number of transmissions is two is low. The difference between two configurations, taking the percentage difference of the two mean values, is 14% for maximum filtering and 12% for minimum filtering, meaning that the diffuse light intensity is, on average, reduced by 12–14% by the presence of upper and lower eyelashes. In these figures, we can better appreciate the effect of the filter and how the two configurations (with and without the eyelashes) have changed. The action of the filter is not constant over the cornea surface. Although the maximum values of diffuse radiation view factor are in the central-temporal part of the cornea in the configuration without eyelashes, the filtering effect decreases these values in the configuration with eyelashes. The greatest value of filtering (20–24%) in the central-temporal and central-nasal part together with the action of the filter make the region around the center of the cornea the area with the maximum value of diffuse radiation view factor. Plus, in this configuration, the less protected is the cornea center, whereas the most protected parts are the border regions, especially upper ones.

In Fig. 8 some sensitivity experiments are shown with different eyelashes parameters. In this second experiment a particular eyelashes length (for upper and lower eyelashes) has been chosen and then the percentage difference has been computed (y-axis) for different values of the ratio d/h (x-axis). Percentage difference is computed between the configuration with and without the eyelashes. For each length, a coloured region delimited by two curve is shown: the upper curve is obtained from the configuration with eyelashes with maximum filtering (α_{max}), and the lower curve is obtained from the configuration with eyelashes with minimum filtering (α_{min}). Filtering amplitude increases with the length and with the increment of the ratio d/h. A value of $d/h = 1$ means that all radiation passing through the eyelashes is transmitted and absorbed in the case of minimum filtering and completely blocked in the case of maximum filtering. A value of $d/h = 0$ means that the eyelashes are completely transparent and no filtering effect is applied. These results show that the trend is a monotonic function similar to a logarithm. This trend is similar for different length of eyelashes, without overlap between the filtering efficiency curves. As expected, for a fixed value of d/h the filtering amplitude increases with length. Filtering effect could be also the same for different eyelashes parameters. For example, for an upper eyelash length of 5 mm and a ratio of $d/h = 0.45$, the filtering is essentially the same for a length of 6 mm and a ratio of $d/h = 0.3$. It does not mean however that the filtering effect is spatially the same in both situations, since it is an average value.

Table 2
Summary of average values used for a typical eyelash.

component	value
upper eyelashes length	7 mm
lower eyelashes lengtt	5 mm
d	65 μm
h	0.143 mm
d/h	0.455

7. Discussion

Dividing the measurement of filtering effect of eyelashes in two parts has allowed to determine the amplitude of the filter itself and all parameters that can affect it. The filter (Equation (9)) shows an amplitude variable with light direction (θ and ϕ) and structural parameters of eyelashes (diameter d and center-to-center distance h) as it was supposed to.

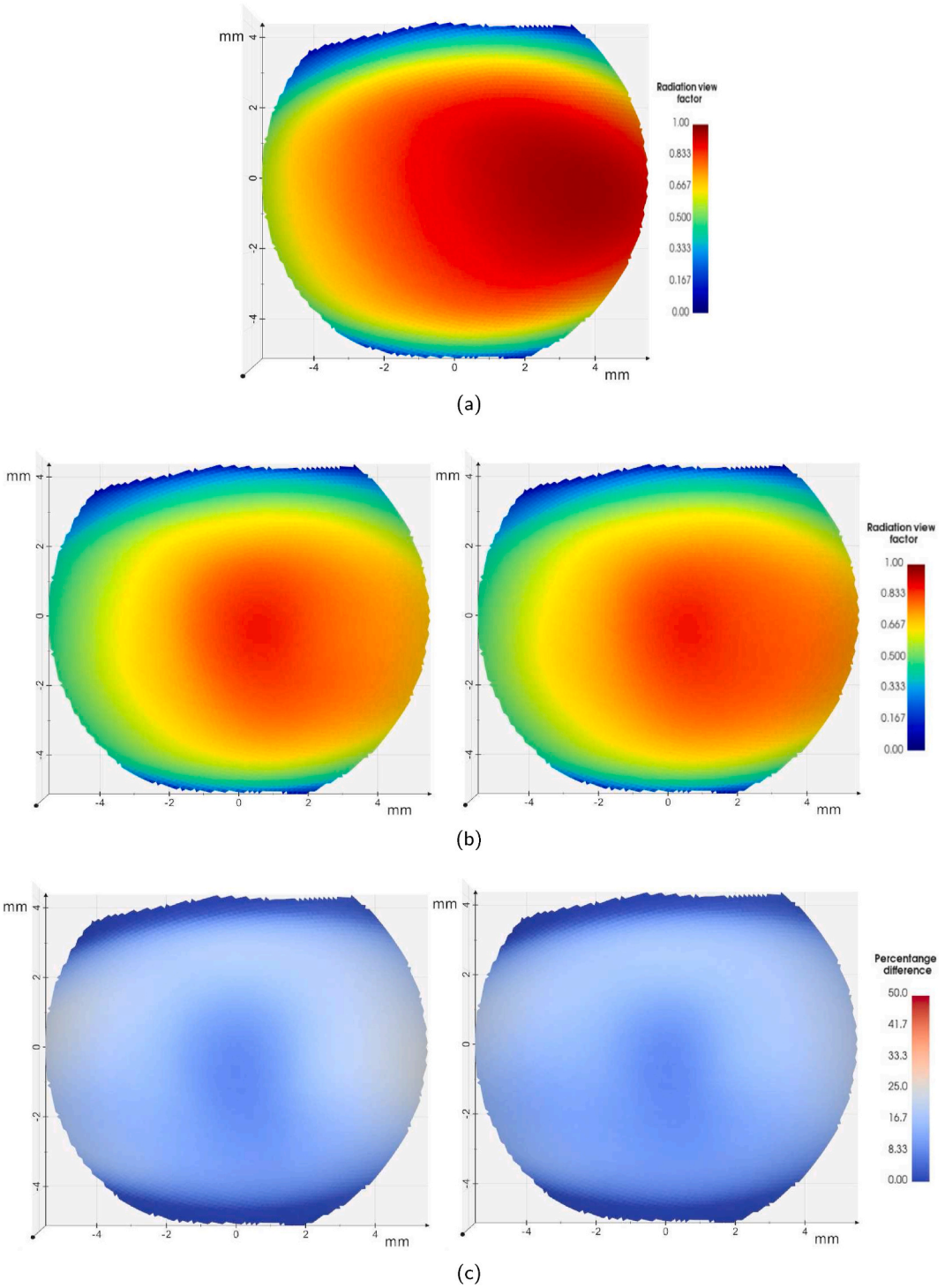

Fig. 7. Figure (a): frontal vision of the diffuse radiation view factor for the head-model left-cornea without eyelashes. Figure (b): frontal vision of the diffuse radiation view factor for the head-model left-cornea with eyelashes by using α_{max} and α_{min} on the left and right figure, respectively (e.g. $\alpha = 0$ and $\alpha = k_T$ for $|\beta_{\theta,\phi}| > \cos^{-1}(d/h)$). Figure (c): filtering percentage difference calculated from the results from Figure (a) and the corresponding results of Figures (b).

Eyelashes have been designed on the head model using lengths found in the literature. Their shape follows the eyelid curve and the orientation is always $\pi/2$, with respect to the vertical. In reality, the eyelashes are composed by different layers, even though the data found in the literature often reports a single density value (an average value). With different layers, density could be increased and could furthermore rise the level of filtering, changing the form of Equation (9). Plus, cilia lengths change along the eyelash profile [36]. The maximum length of eyelashes is around the center, while the minimum one is in the temporal region. This length variation might change the distribution of the diffuse radiation view factor obtained. It is conceivable that a shorter length could reduce the filtering effect in the central-temporal region of the cornea, whereas a longer length in the center could increase the filtering effect around the center of the cornea, making the general filtering effect on the cornea even more uniform than observed. The orientation of the eyelashes might be another source of discrepancy.

As mentioned in section 3.2, results are unique for a unique type of head. Discrepancies in results can be caused by eyelid and forehead

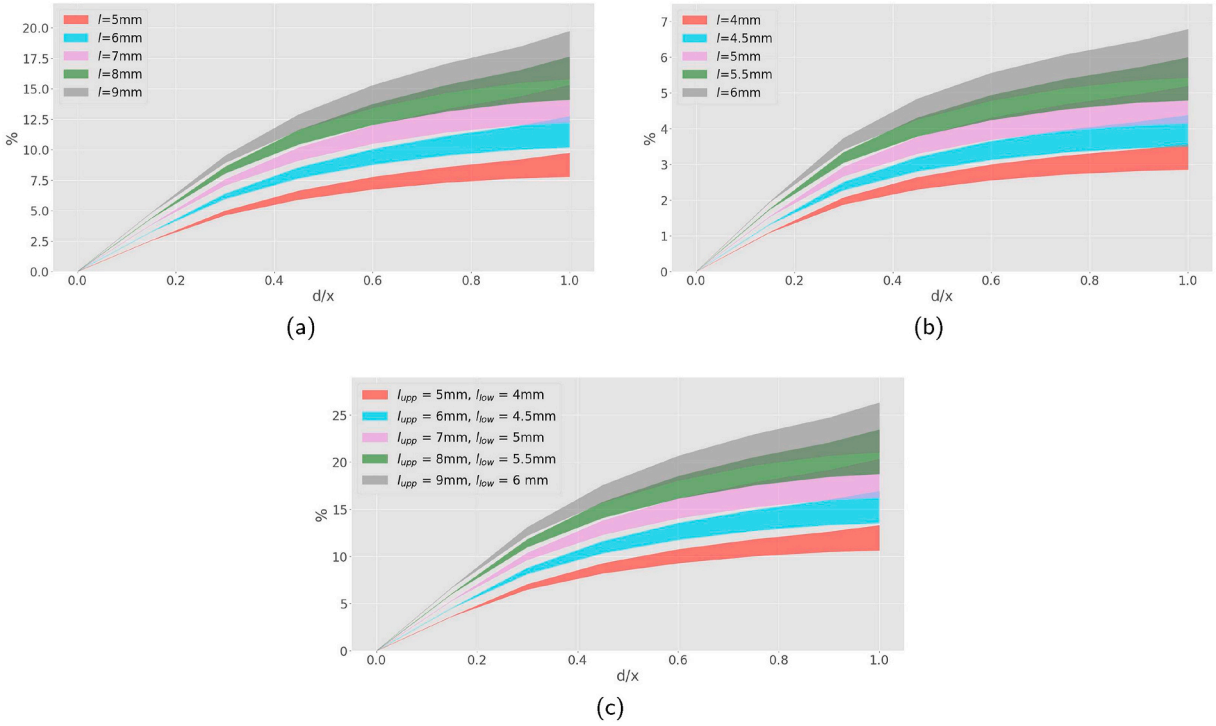

Fig. 8. Sensitivity results for the filtering effect in percentage (%) with different eyelashes parameters (x axis: ratio d/h, y axis: percentage difference). Each coloured region is delimited by two curves: the upper curve, obtained using α_{max}, and the lower curve, obtained using α_{min}. Figure (a): difference computed for different upper eyelashes length (without lower eyelashes). Figure (b): difference computed for different lower eyelashes length (without upper eyelashes). Figure (c): difference considering both variations in upper and lower eyelashes.

prominence, nose and cheek shape (which can put in shadow a little part of the cornea). With Equation (9) it is now possible to compute these differences by taking several head models to understand what the filtering amplitude is.

Another interesting point would be to investigate the filtering amplitude with natural light. In this way, filtering effect depends on the direction of direct light, changes with location, season, weather, etc. Thus, there will be a percentage difference value for each set of these variables.

8. Conclusion

This work shows how ultraviolet radiation received by human eyes can be reduced by a tiny layer of opaque fibers. Light reduction depends on both dimension and orientation of fibers and direction of incoming light. Longer fibers have stronger filtering power and the filtering power changes with distance and dimension of fibers. For the values found in the literature (diameter, center-to-center distance and length of cilia) and a simple structural model, the average filtering effect provided by the eyelashes is estimated to be around 12–14% compared to same condition without eyelashes.

Declaration of competing interest

The authors declare that they have no known competing financial interests or personal relationships that could have appeared to influence the work reported in this paper.

Acknowledgments

This research is developed within the framework of the InExES project: "Coupling Internal and External Eye Simulation for a better prediction of natural and artificial light exposure (Internal and External Eye Simulation)" which is financially supported by the Velux Stiftung in Zürich, Switzerland.

References

[1] Julio Martín-Moro, J. Castillo, New theories on the role of the eyelashes. a fourth layer in the tear film? Arch. Soc. Esp. Oftalmol. 90 (2015) 405–406, 09.
[2] Guillermo J. Amador, Wenbin Mao, DeMercurio Peter, Carmen Montero, Joel Clewis, Alexeev Alexander, L. David, Hu, Eyelashes divert airflow to protect the eye, J. R. Soc. Interface 12 (105) (2015) 20141294.
[3] Siyu Zou, Jinping Zha, Jie Xiao, Xiao Dong Chen, How eyelashes can protect the eye through inhibiting ocular water evaporation: a chemical engineering perspective, J. R. Soc. Interface 16 (159) (2019) 20190425.
[4] Graham R. Martin, Hendri C. Coetzee, Visual fields in hornbills: precision-grasping and sunshades, Ibis 146 (1) (2004) 18–26.
[5] Neri Pucci, Elio Novembre, Enrico Lombardi, Cristina Massai, Roberto Bernardini, Roberto Caputo, Luciana Campa, Cinzia Libero, Vierucci Alberto, Long eyelashes in a case series of 93 children with vernal keratoconjunctivitis, Pediatrics 115 (2005) e86–91, 02.
[6] J.P.G. Bergmanson, P.G. Söderberg, The significance of ultraviolet radiation for eye diseases. a review with comments on the efficacy of uv-blocking contact lenses, Ophthalmic Physiol. Opt. 15 (2) (1995) 83–91.
[7] Hiroshi Sasaki, Yasuo Sakamoto, Cristina Schnider, Nobuyuki Fujita, Natsuko Hatsusaka, David Sliney, Kazuyuki Sasaki, Uv-b exposure to the eye depending on solar altitude, Eye Contact Lens 37 (2011), 191–5, 07.
[8] Bradley Smith, Shaleen Belani, Ho Allen, Ultraviolet and near-blue light effects on the eye, Int. Ophthalmol. Clin. 45 (2005), 107–15, 02.
[9] Alfio V. Parisi, Don Smith, Peter Schouten, David J. Turnbull, Solar ultraviolet protection provided by human head hair, Photochem. Photobiol. 85 (1) (2009) 250–254.
[10] A.V. Parisi, D.J. Turnbull, N. Downs, D. Smith, Dosimetric investigation of the solar erythemal UV radiation protection provided by beards and moustaches, Radiat. Protect. Dosim. 150 (3) (2011) 278–282, 11.
[11] Maria de Galvez, Jose Aguilera, Jean-Luc Bernabo, Cristina Sanchez-Roldan, Enrique Herrera-Ceballos, Human hair as a natural sun protection agent: a quantitative study, Photochem. Photobiol. 91 (2015), 02.
[12] David Turbert, The Sun, UV Light and Your Eyes, american academy of ophthalmology, 2021.
[13] Manoj Kumar Gupta, Kuldip J. Bumtariya, H.A. Shukla, Pranav Patel, Ziauddin Khan, Methods for evaluation of radiation view factor: a review, Mater. Today Proc. 4 (2, Part A) (2017) 1236–1243, 5th International Conference of Materials Processing and Characterization (ICMPC 2016).

[14] David Vernez, Milon Antoine, Laurent Francioli, Jean-Luc Bulliard, Laurent Vuilleumier, Laurent Moccozet, A numeric model to simulate solar individual ultraviolet exposure, Photochem. Photobiol. 87 (2011) 721–728, 05.
[15] Arianna Religi, Laurent Moccozet, Meghdad Farahmand, Laurent Vuilleumier, David Vernez, Milon Antoine, Jean-Luc Bulliard, Claudine Backes, Simuvex v2: a numeric model to predict anatomical solar ultraviolet exposure, in: 2016 SAI Computing Conference, SAI), 2016, pp. 1344–1348.
[16] Paolo Cignoni, Marco Callieri, Massimiliano Corsini, Matteo Dellepiane, Fabio Ganovelli, Ranzuglia Guido, MeshLab: an open-source mesh processing tool, in: Vittorio Scarano, Rosario De Chiara, Ugo Erra (Eds.), Eurographics Italian Chapter Conference, The Eurographics Association, 2008.
[17] Alexander V. Goncharov, Chris Dainty, Wide-field schematic eye models with gradient-index lens, J. Opt. Soc. Am. A 24 (8) (Aug 2007) 2157–2174.
[18] C. Erb, F. Rüfer, A. Schröder, White-to-white corneal diameter: normal values in healthy humans obtained with the orbscan ii topography system, Cornea 24 (Apr 2005).
[19] Willem Bosch, Ineke Leenders, Paul Mulder, Topographic anatomy of the eyelids, and the effects of sex and age, Br. J. Ophthalmol. 83 (1999), 347–52, 04.
[20] E Becker Sebastien Thibaut, Laurence Caisey, Diane Baras, S. Karatas, O. Jammayrac, Pierre Pisella, Bruno Bernard, Human eyelash characterization, Br. J. Dermatol. 162 (2009), 304–10, 09.
[21] Sarah Aumond, Etty Bitton, The eyelash follicle features and anomalies: a review, J Optometry 11 (2018), 07.
[22] Xiyong Huang, Michael Protheroe, Ahmed Al-Jumaily, Sharad Paul, Andrew Chalmers, Review of human hair optical properties in possible relation to melanoma development, J. Biomed. Opt. 23 (1) (2018), 05.
[23] Xiyong Huang, Michael D. Protheroe, M. Ahmed, Al-Jumaily, Sharad P. Paul, Andrew N. Chalmers, Shuao Wang, Juan Diwu, Wei Liu, Contribution of human hair in solar uv transmission in skin: implications for melanoma development, Ann. Biomed. Eng. 47 (2019) 2372–2383.
[24] Yuta Miyamae, Yumika Yamakawa, Yukihiro Ozaki, Evaluation of physical properties of human hair by diffuse reflectance near-infrared spectroscopy, Appl. Spectrosc. 61 (2007), 212–7, 03.
[25] Donald J. Lyman, Paula Schofield, Attenuated total reflection fourier transform infrared spectroscopy analysis of human hair fiber structure, Appl. Spectrosc. 62 (5) (May 2008) 525–535.
[26] Stephen R. Marschner, Henrik Wann Jensen, Mike Cammarano, Steve Worley, Pat Hanrahan, Light scattering from human hair fibers, ACM Trans. Graph. 22 (3) (July 2003) 780–791.
[27] Eugene d'Eon, Guillaume François, Martin Hill, Letteri Joe, Jean-Marie Aubry, An energy-conserving hair reflectance model, Comput. Graph. Forum 30 (2011) 1181–1187, 06.
[28] Pramook Khungurn, Steve Marschner, Azimuthal scattering from elliptical hair fibers, ACM Trans. Graph. 36 (2) (April 2017).
[29] Leonid B. Pekelis, Christophe Hery, Ryusuke Villemin, Junyi Ling, Pixar, A Data-Driven Light Scattering Model for Hair, 2015.
[30] A.C.S. Nogueira, L.E. Dicelio, I. Joekes, About photo-damage of human hair, Photochem. Photobiol. Sci. 5 (2006) 165–169.
[31] Ana Carolina Santos Nogueira, Ines Joekes, Hair color changes and protein damage caused by ultraviolet radiation, J. Photochem. Photobiol. B Biol. 74 (2) (2004) 109–117.
[32] Simone Liberini, Antonio Avolio, Stevn Thomas Yankowski, Alessandro Rizzi, Consistency issues in hair spectral reflectance and colour measurements, Color. Technol. 136 (3) (2020) 244–254.
[33] A.O. Natarova, Nikolay Kokodii, Stanislav Pogorelov, I.A. Priz, Physical Methods of Analysis of the Human Hair Properties, 2019, pp. 1–6, 09.
[34] Robert Osada, Thomas Funkhouser, Chazelle Bernard, David Dobkin, Shape distributions, ACM Trans. Graph. 21 (4) (October 2002) 807–832.
[35] Gervasio Pineiro, Susana Perelman, Juan P. Guerschman, José M. Paruelo, How to evaluate models: observed vs. predicted or predicted vs. observed? Ecol. Model. 216 (3) (2008) 316–322.
[36] Na Jung-Im, Ohsang Kwon, B.J. Kim, W.S. Park, J.K. Oh, Kyu Han Kim, Kyu-Woan Cho, H.C. Eun, Ethnic characteristics of eyelashes: a comparative analysis in asian and caucasian females, Br. J. Dermatol. 155 (2007), 1170–6, 01.
[37] Mamoru Kikuchi, Ken Matsuda, Yasuhiro Ishihara, Tetsu Yanai, Kiyoto Yasuta, Hosokawa Ko, Tetsuji Uemura, A study of normal eyelashes in Japanese individuals, Global Dermatology 2 (2015) 74–77, 02.
[38] Hironori Tohmyoh, Mitsuharu Ishihara, Kaori Ikuta, Tomoko Watanabe, On the correlation between the curvature of the human eyelash and its geometrical features, Acta Biomater. 76 (2018) 108–115.